TURBULENT BOUNDARY LAYERS OVER MULTISCALE ROUGH PATCHES

Christina Vanderwel

Faculty of Engineering and the Environment
University of Southampton
Southampton, S017 1BJ, UK
c.m.vanderwel@soton.ac.uk

Bharathram Ganapathisubramani

Faculty of Engineering and the Environment
University of Southampton
Southampton, S017 1BJ, UK
g.bharath@soton.ac.uk

ABSTRACT

In this work, we experimentally investigate the effects of multiscale rough patches on the drag and flow structure of a fully rough turbulent boundary layer in a wind tunnel. Several patches containing both organised and randomised arrangements of cubes of multiple sizes were tested in order to study the dependence of drag on the frontal solidity of the patch. One of the patches was also replicated with some of the sizes of cubes deleted in order to ascertain the importance of each scale of roughness. The drag of each patch was measured with a drag balance for a range of Reynolds numbers. Flow fields in several cross-sections were captured using PIV. Maps of the velocity deficit and increased turbulence activity in the wake of the patches were determined and used to define the extent of the internal boundary layer formed by each patch.

INTRODUCTION

Flows over rough surfaces are extremely common in environmental and engineering applications. Examples include the winds that flow over rural and urban landscapes or the flow of water around a moving ship hull. In these applications, the accurate prediction of the drag and structure of the turbulent boundary layer that develops along the surface is critically important. Turbulent boundary layers are known to be sensitive to the geometry of the wall roughness; however, most previous studies of the effects of surface roughness have focussed on surfaces with homogenous roughness. In this study, we investigate the effect of finite patches of multiscale obstacles on the drag and flow structure. Multiscale patches appear in many engineering applications including the drag from barnacles on a ship hull (e.g. Barros et al., 2016), the effect of river vegetation on turbulence and sedimentation (e.g. Hepf, 2012), and weather prediction in urban canopies (e.g. Grimmond and Oke, 1999).

A patch of roughness is expected to exhibit similar qualities as abrupt changes in surface roughness, such as smooth-to-rough and rough-to-smooth transitions, which have been studied in depth previously (Antonia & Luxton, 1971; Hanson & Ganapathisubramani, 2016). The effects of changing surface roughness are typically modelled by determining the extent of the internal boundary layer, which is formed at the interface of the surface change, and which marks the boundary where the effects of the surface no longer affect outer layer similarity (Mahrt, 2000; Bou-Zeid et al., 2006).

When considering patches containing distinct obstacles, such as cubes or cylinders, the solidity of the surface has been highlighted as an important parameter (Placidi & Ganapathisubramani, 2015). In addition to solidity, the importance of the arrangement of the structures has also been highlighted, as it can cause 'shielding' of downstream structures (Yang et al., 2016). The solidity of a patch can also influence the vortex structures that develop in the wake and at the edges of the patch (Hepf, 2012).

In this study, we extend this line of research to study finite patches of multiscale cubes, concentrating on the effects of the patch arrangement on the drag and flow structure. We considered two different parameters: (1) the effect of frontal solidity and (2) the significance of the multiscale features.

In the first study, we designed patches with equal planform solidities λ_P (defined as the fraction of the planform area that is covered by cubes), but with varying frontal solidity λ_F (defined as the sum of forward-facing faces normalised by the planform area; Grimmond and Oke, 1999). In this way, for surfaces consisting of only cubes, λ_P and λ_F will only differ if cubes touch each other, hence this difference is an indicator of shielding.

In the second study, we replicated one of the patches several times with some of the scales of cubes deleted in order to study the contributions of each scale of roughness. The intent is to determine the minimum resolution required to properly resolve flows over complex features, which is important for computational modellers.
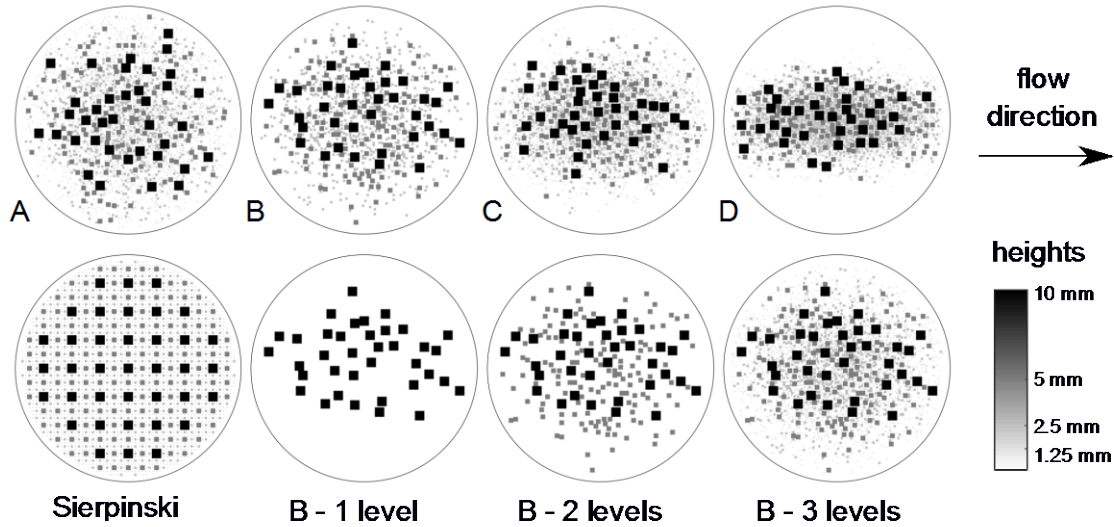
1

Figure 1. The planform views of the different test patches.

DESIGN OF THE PATCHES

Many features of nature exhibit fractal properties, including the height distribution of eroded surfaces and the layout of urban sprawl (Mandelbrot, 1983). For this reason, our test cases were modelled using idealised fractal patterns. The designs of the multiscale patches were inspired by the Sierpinksi carpet fractal pattern. The Sierpinski carpet is a plane fractal that comprises grids of squares of diminishing sizes. In order to create a 3D patch of roughness from the Sierpinksi carpet, each square in the pattern was extruded into a cube. Four iterations of the fractal were included so that the patch included four different sizes of cubes (10, 5, 2.5, 1.25 mm). The number of each size of cube followed as near as possible to a power-law distribution (37, 140, 536, and 1884 cubes of each size, respectively) so the surface area covered by each scale was roughly equal. The patch was confined to a radius of $r = 120$ mm and 3D printed in polyamide resulting in a smooth texture and good resolution of even the smallest cubes. A 3D model of this patch is presented in figure 2, while planform views of this and the other patches in the study are presented in figure 1.
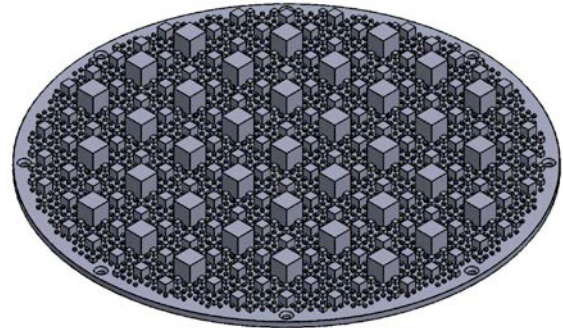
In the first part of the study, in order to study the effect of the arrangement of the cubes, in addition to the regular Sierpinksi pattern, four additional patches were constructed using random arrangements of the same number of cubes. The random distributions were designed in such a way as to vary σ_z, the second central moment of the arrangement in the spanwise direction, and therefore the frontal solidity λ_F of each patch. As λ_F is defined as the sum of forward-facing faces normalised by the planform area (Grimmond and Oke, 1999), this represents the amount of 'shielding' that occurs – the narrowest layout (D) has the fewest forward facing faces and therefore the smallest λ_F. Because the Sierpinski layout has no touching faces, it has the maximum value of λ_F. However, because these patches all comprised the same number of cubes, each of these patches had the same planform solidity of $\lambda_P = 0.298$. Maps of the different arrangements are presented in figure 1 and their properties are shown in table 1.

Figure 2. 3D model of the Sierpinski carpet patch.

Patch	σ_z / r	λ_P	λ_F
Sierpinski	0.45	0.298	0.298
Layout A	0.38	0.298	0.254
Layout B	0.32	0.298	0.241
Layout C	0.27	0.298	0.232
Layout D	0.20	0.298	0.203
B - 3 levels	0.32	0.233	0.205
B - 2 levels	0.32	0.159	0.150
B - 1 level	0.27	0.082	0.080

Table 1. Properties of the patches.

In the second part of the study, in order to study the contribution of each of the different scales, one of the randomised patches (layout B) was replicated three additional times with reduced number of scales each time. By this we mean one replicated patch included only the 10, 5, and 2.5 mm cubes, while another included only the 10 and 5mm cubes, and the last included only the largest 10 mm cubes. In this way, we hope to decompose the contributions of each scale to the total drag and flow structure of the patch. Maps of the different arrangements are also presented in figure 1.
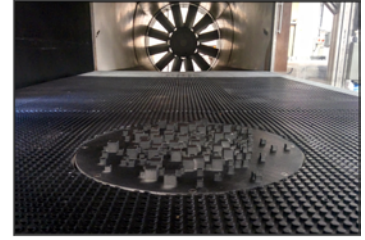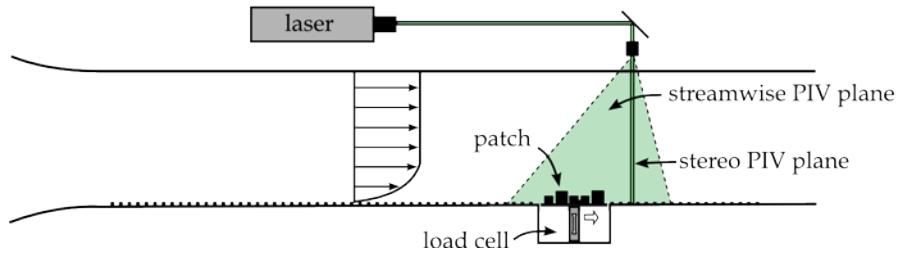
2

Figure 3. Schematic of the experimental setup and a photograph of the patch installed the wind tunnel.

EXPERIMENTAL DETAILS

Experiments were conducted in a suction windtunnel at the University of Southampton that has a test section that is 4.5 m long and a 0.9 m $\times$ 0.6 m cross-section. A turbulent boundary layer was created on the floor of the tunnel, which was covered with homogeneous roughness created by Lego baseboards made of bumps with a height of 1.7 mm (Placidi and Ganapathisubramani, 2005; Vanderwel and Ganapathisubramani, 2014). The patches were placed 4 m downstream of the leading edge of the baseboards where the boundary layer thickness was $\delta = 85$ mm, given a freestream velocity of $U_\infty = 20$ m/s. At this point, the incoming boundary layer was fully rough for all the wind speeds considered here. As the maximum height of all patches was H = 10 mm this means the patches were well-immersed in the boundary layer (H/δ = 0.12).

The drag of the patches was measured using a floating element drag balance. The balance measured forces using multiple Tedea-Huntleigh model 1004 load sensors connected to a National Instruments PXIe-1062Q DAQ. The sensors were calibrated by hanging known weights on a string connected to the floating element through a pulley. The measurements were repeated three times for each patch and the uncertainty (including sensitivity and repeatability) of the load measurements was estimated to be ± 0.8 g, which was an order of magnitude smaller than the magnitude of the measured drag.

The flow fields in two cross-sections of the flow were captured using conventional planar and stereoscopic particle image velocimety (PIV) respectively. Measurements in a streamwise-vertical plane aligned with the patch centre were acquired using two side-by-side LaVision Imager Pro LX 16M cameras. The vector fields from the two cameras were then stitched together to create a long field of view that captured the incoming flow ahead of the patch and extended well into the wake of the patch. Subsequently, measurements of the patch wake were acquired in a plane located 63 mm downstream of the edge of the patch, using the same cameras placed in a stereoscopic configuration. For each case, 1000 image pairs were acquired at a rate of 0.7 Hz. The light sheet was created by two synchronised Litron 200-15PIV Nd:YAG lasers that were in each case aligned using mirrors to form a single light sheet. The flow was seeded using a Magnum 1200 smoke machine. Vector fields were calculated using LaVision DaVis 8 resulting in a resolution of roughly one vector per millimeter in both configurations.

RESULTS
Drag measurements

The drag of each patch was measured at four different wind speeds ranging from $U_\infty = 15$-30 m/s and repeated three times for each case. Defining the Reynolds number as $Re_L = UL/\nu$, where L is the fetch of the incoming boundary layer and ν is the kinematic viscosity of air, this results in a range of $3.9 \times 10^6 < Re_L < 7.7 \times 10^6$. The measurements are presented in figure 4a. The measured drag ranged between 20-35 g at the top wind speed, and the differences between the drag of the different patches was significantly greater than the measurement uncertainty. For each patch, the measured drag increased with wind speed following a power law as $F_D = a\,Re_L^n$, where $n = 2.0 \pm 0.1$ as would be expected if the coefficient of drag was constant. The drag coefficient of each patch was defined as

$$C_D = \frac{F_D}{\frac{1}{2}\rho U_\infty^2 A_P}$$

where $A_P = \pi r^2$ is the planform area of the patch. The values of C_D are presented in figure 4b and were nearly constant for each case, varying by less than 3% over the range of tested Reynolds numbers. This suggests that the flow phenomena does not drastically change with Reynolds number. This is typical of turbulent flows around features with sharp edges such as cubes, as the sharp edge fixes the separation point; a laminar flow, on the other hand, might produce vortex shedding which is sensitive to the wind speed.

Comparing the drag measurements of the different randomised arrangements, the results show a monotonic increase in drag with increasing frontal solidity. This is consistent with the idea that the 'shielding' of downstream elements can significantly reduce drag. What is interesting is that the drag of the orderly Sierpinski carpet arrangement, which has the highest frontal solidity, produced a drag comparable to Layout A, which had a lower λ_F, but the highest λ_F of the randomised arrangements. This suggests that frontal solidity alone is insufficient to predict drag, especially when the surface structure is organised in some way rather than randomised. In the special case of the Sierpinksi carpet arrangement, many alleyways are left exposed for air to flow through, making the flow act in a similar way to a patch with less solidity.

The drag was also measured without the patch installed in order to estimate the contributions of the pressure drag and the additional skin friction from the cubes. As shown in figure 4, the drag with no patch and just a continuation of the rough surface was roughly half the magnitude of those of the patches,
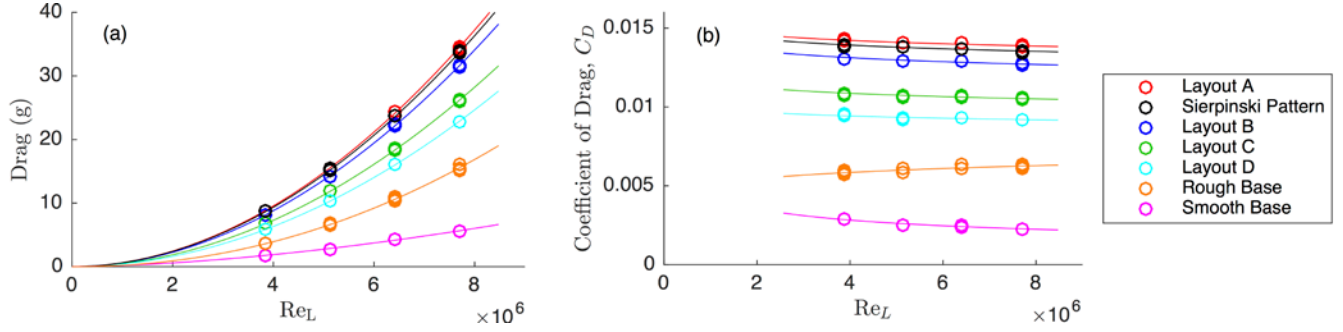
3

Figure 4. (a) Drag measurements of the five patches compared with baseline measurements of the rough baseboard and of a smooth plate. (b) The corresponding coefficients of drag.

demonstrating that the presence of the cubes was indeed significant. The drag of a smooth patch was also measured for comparison, and was found to be half again of the drag of the rough surface. These values are used as baselines for the second part of the study to be discussed in a later section.

Velocity fields

The velocity fields were captured in two cross-sections of the flow for each patch, all with a freestream velocity of $U_\infty = 20$ m/s ($Re_L = 5.1 \times 10^6$). As the drag coefficients of each patch were fairly independent of wind speed, we expect the flow patterns measured at this speed to be representative. The velocity maps confirmed that the incoming boundary layer had a thickness of $\delta = 85$ mm. Examples of typical instantaneous velocity maps acquired in both measurement planes are presented in figure 5.

In order to distinguish the impact of the patch, the average velocity deficit in the vicinity of the patch was computed as

$$\Delta U = \overline{U} - \overline{U}_{\mathrm{ref}}$$

where $\overline{U}$ is the average velocity field and $\overline{U}_{\mathrm{ref}}$ is the velocity map measured using the rough base without any patch. Figure 6a shows an example map of this velocity deficit. The internal boundary layer created by the patch was defined as the contour line corresponding with a velocity deficit of $\Delta U/U_\infty = 1\%$. For all the patches, the internal boundary layer did not extend beyond 3-4 H from the floor, indicating that the patches did not affect similarity in the outer region of the boundary layer. The exception to this was a relatively large region at the leading edge of the patch due to the initial deflection of the flow around the patch, but which didn't seem to influence the wake that formed downstream. In each case, the wakes extended several radii downstream. The length of the wake, L_w, was defined as the

Patch	λ_F	F_D (g)	ΔM (g)	L_w/r
Sierpinkski	0.298	15.3	5.6	2.13
Layout A	0.254	15.6	6.4	1.83
Layout B	0.241	14.4	6.1	1.63
Layout C	0.232	11.9	4.2	2.08
Layout D	0.203	10.3	3.7	2.19

Table 2. Properties of the patches measured at $Re_L = 5.1 \times 10^6$: the drag balance measurement, F_D, the momentum deficit, ΔM, converted to grams, and the lengths of the wakes, L_w.

distance from the trailing edge of the patch to the point where the velocity deficit in the wake recovered to 10% of U_∞. Results are summarised in table 2. In general, the wakes of the narrower patches extended farther downstream, with the wake of the narrowest patch (D) extending roughly 20% farther than that of the widest patch (A). This indicates that although the wider patches create more drag, the denser narrower patches create more focused disturbances to the flow that take longer to recover.

To visualise the impact of each patch on the turbulent kinetic energy in the flow, the additional vertical velocity fluctuations created by the patch was defined as

$$\Delta u' = u' - u'_{\mathrm{ref}}$$

where u' denotes the root-mean-square streamwise velocity fluctuations and u'_{ref} is the background level of u' present without any patch installed. An example map is presented in figure 6b. The results indicated increased turbulent activity in the wake of each patch compared with having no patch, the extent of which was consistent with the edge of the internal boundary layer identified by the velocity deficit.

Maps of the average velocity deficit downstream of each of the patches are presented in figure 7. As a second indication of the drag of the patch, the momentum deficit in the spanwise cross-section located downstream of the patch was calculated as

$$\Delta M = \rho \iint \overline{U}(\overline{U}_{\mathrm{ref}} - \overline{U}) \mathrm{d}y \mathrm{d}z.$$

The results are presented in table 2. When converted into grams, it is apparent that the momentum deficit only accounts for a fraction of the total drag measured by the drag balance; however, this discrepancy is a result of the fact that the measurement plane is in the near field where the pressure would not have fully recovered to the upstream value. Nevertheless, the momentum deficits follow similar trends as the drag measurements: the wider patches created larger wakes and therefore more drag. Once again, the exception is the Sierpinksi pattern, which had less momentum deficit and a longer wake than the randomised layouts with similar solidity. While the alleyways left open in the regular Siepinski layout resulted in a weaker wake and hence less momentum drag, they clearly were also not conducive to the kinds of flow structures that help a wake recover, resulting in a longer wake. This highlights the fact that organised arrangements cannot be treated in the same general manner as randomised surfaces.
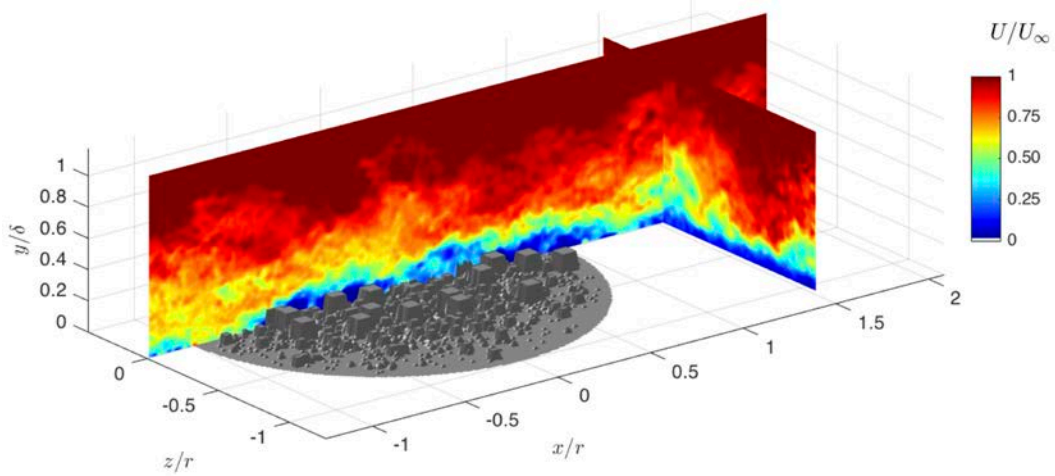
4

Figure 5. Examples of the instantaneous velocity fields over patch B.
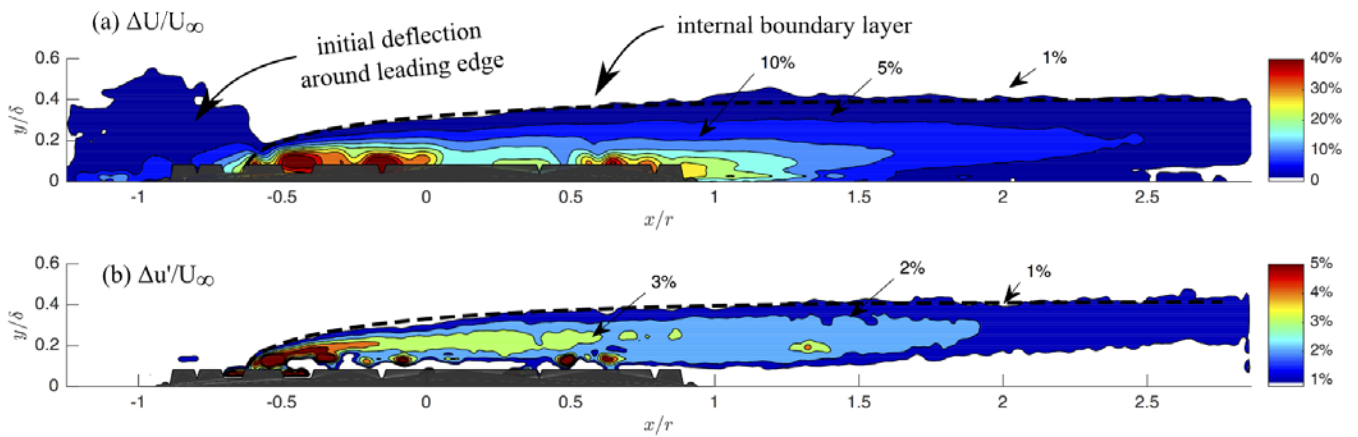

Figure 6. (a) Map of the average velocity deficit ΔU created by the presence of patch B when compared with the flow field with no patch. The 1% contour identifies the edge of the internal boundary layer, with the exception of a localised region around the leading edge of the patch where the flow initially deflects around the patch. (b) Map of the average additional turbulent kinetic energy around patch B. The 1% contour coincides with the edge of the internal boundary layer.
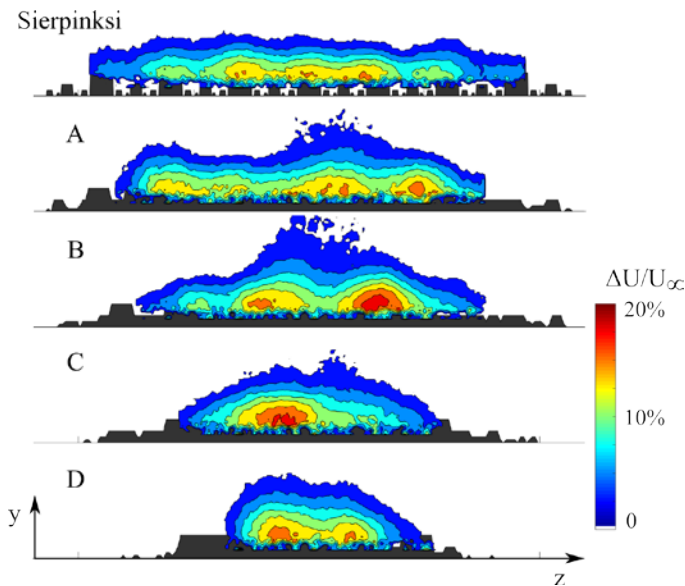

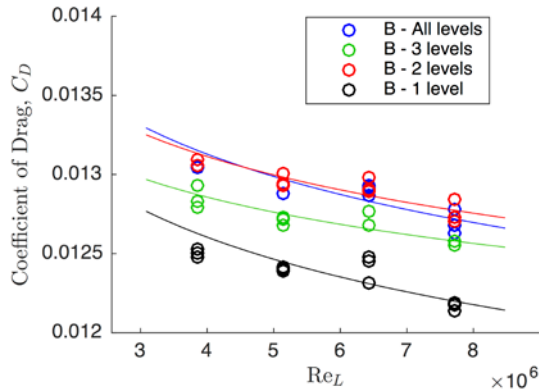Figure 7. Maps of the average velocity deficit downstream of each of the patches.

5

Figure 8. Drag coefficient of Layout B constructed with diminishing numbers of scales.
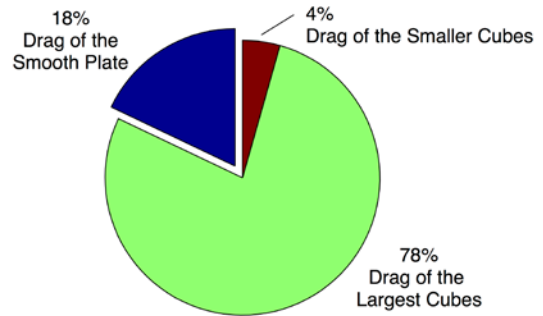

Figure 9. Decomposing the contributions to drag of Layout B: 78% of the drag comes from the 10 mm cubes, whereas only 4% is attributed to the combined effect of the 5, 2.5, and 1.25 mm cubes.

Significance of the different scales

The drag measurements of Layout B replicated with different numbers of scales are presented in figure 8. The difference in the drag of the complete patch and the one containing only the largest size of cubes was only approximately 5%, indicating that the addition of the smaller scales appears to be minimal. The PIV measurements also showed that the wakes of the patches with different numbers of cubes were essentially indiscernable.

The contributions of the different sources of drag are broken down in figure 9. As we showed previously, the drag of the smooth surface was only 18% of the value of the total drag of Layout B. When the largest cubes were added, the measured drag shot up to 96% of the final value, indicating that these scales are responsible for the majority (78%) of the total drag. Finally, the three smaller scales of cubes only contributed about 4% of the total drag. This simplistic decomposition is particularly crude as it assumes that the effects of each scale of cube are cumulative and neglects any coupling (such as sheilding) that occurs. In particular, it does not explain how the drag of the layout with three levels is less than the layout with only two; this must be attributed to the sheilding effects of the 2.5 mm cubes. However, the fact that the drag of layouts did not differ significantly is good news for computational modellers, as this suggests that a very fine resolution of the surface texture features is not necessary to get reasonable predictions of the drag.

CONCLUSIONS

In summary, the drag and flow structure of finite multiscale patches were measured. In all cases, the internal boundary layers created by the patches were much thinner than the boundary layer thickness, indicating that the patches did not affect similarity in the outer layer. The results indicated that the drag of the randomised patches increased monotonically with increasing frontal solidity, illustrating how "shielding" can reduce drag. Furthermore, we showed that the majority of the drag is attributed to the largest scales of roughness. We also found that the patch that was organised as a Sierpinski pattern did not fit the same trend as the randomized arrangements, highlighting how exposed alleyways through the patch can significantly affect the flow.

REFERENCES

Antonia, R. A., and R. E. Luxton. "The response of a turbulent boundary layer to a step change in surface roughness Part 1. Smooth to rough." *J. Fluid Mech,* 48.4: 721-761, 1971.

Barros, J.M., Murphy, E.A., Schultz, M.P. "Particle Image Velocimetry Measurements of the Flow over Barnacles in a Turbulent Boundary Layer," *18th Int. Symp. on the Application of Laser and Imaging Techniques to Fluid Mechanics*, Lisbon, Portugal, July 4-7, 2016.

Bou-Zeid, E., Meneveau, C. and Parlange, M.B. "Large-eddy simulation of neutral atmospheric boundary layer flow over heterogeneous surfaces: Blending height and effective surface roughness." *Water Resources Research,* 40.2, 2004.

Grimmond, C.S.B., and Oke, T.R. "Aerodynamic properties of urban areas derived from analysis of surface form," *J. Applied Meteorology*, 38:9, 1262-1292, 1999.

Hanson, R.E. and Ganapathisubramani, B., "Development of turbulent boundary layers past a step change in wall roughness," *J. Fluid Mech*, 795, pp. 494-523, 2016.

Mahrt, L. "Surface heterogeneity and vertical structure of the boundary layer." *Boundary-Layer Meteorology,* 96.1-2: 33-62, 2000.

Mandelbrot, B. B., *The fractal geometry of nature*, W. H. Freeman and Company, New York, 1983.

Nepf, H.M. "Hydrodynamics of vegetated channels", *J. Hydraulic Research*, 50:3, 262-279, 2012.

Placidi, M. and Ganapathisubramani, B. "Effects of frontal and plan solidities on aerodynamic parameters and the roughness sublayer in turbulent boundary layers." *J. Fluid Mech,* 782: 541-566, 2015.

Vanderwel, C. and Ganapathisubramani, B. "Effects of spanwise spacing on large-scale secondary flows in rough-wall turbulent boundary layers. " *J. Fluid Mech,* 774:R2, 2015.

Yang, X.I.A., Sadique, J., Mittal, R., and Meneveau, C.. "Exponential roughness layer and analytical model for turbulent boundary layer flow over rectangular-prism roughness elements." *J. Fluid Mech*, 789: 127-165, 2016.

6